JOURNAL OF AIRCRAFT
Vol. 45, No. 6, November–December 2008

Aerodynamic Performances of Battle-Damaged and Repaired Wings of an Aircraft Model

Slimane Djellal*
Polytechnical School, EMP, Bordj-El-Bahri, 16111 Algiers, Algeria
and
Ahmed Ouibrahim†
Mouloud Mammeri University, 15000 Tizi-Ouzou, Algeria

DOI: 10.2514/1.36460

In the tactical schemes of modern air conflicts, where the aircraft is subject to antiaircraft hits, the frequency of operations is very high. The present experimental study concerns two aspects. The preliminary one is devoted to the influence of the simulated gunfire damage on the aerodynamic performance of a typical aircraft model for different sizes and positions of the hole on the wings. The secondary one deals with the recovery of the lost performances by means of damage repairs using patches of different thicknesses and shapes applied at different damage locations (intrados, extrados, and both). The obtained results indicate significant aerodynamic coefficients degradation due to damage, depending on the hole diameter and its spanwise and chordwise position, whereas patch repairs allow one to achieve substantial recovery of the aerodynamic losses in relation with the different aforementioned situations.

Nomenclature

A	=	damage hole surface at the local chord
C_D	=	drag coefficient
C_L	=	lift coefficient
c	=	local wing chord
d	=	hole diameter
e	=	patch thickness
$\bar{e}$	=	relative patch thickness
f	=	fineness
$\bar{f}$	=	relative fineness
S	=	wing surface
α	=	incidence angle
λ	=	taper ratio

Subscripts

damaged	=	result for battle-damaged model
full	=	result for full (both intrados and extrados) repair
lower	=	result for lower surface (or intrados) repair
max	=	maximum
undamaged	=	result for undamaged model
upper	=	result for upper surface (or extrados) repair
ZL	=	value of α for zero lift

I. Introduction

MILITARY aircraft is assumed to operate in a hostile environment, that is, an environment with various operational antiaircraft threats. As a result, the aircraft should be capable of sustaining some kind of battle damage. The survivability of an aircraft is becoming one of the key aircraft design requirements [1] and is dependant upon its vulnerability to damage caused by a variety of threats. The vulnerability assessments generally tend to concentrate only on the structural integrity (reinforcement of the equipment, protection of the vital components, etc.). Few detailed investigations of the aerodynamic effects of damage on the structure, and particularly the wings, have been carried out [2]. Published works to date focus mainly on two-dimensional wings [2,3]. To ensure availability, airplanes must be restored as quickly as possible. This will be accomplished through procedures and repair techniques which are substantially different from those used in times of peace. Successful repairs of battle damage result from quick and accurate assessment, coupled with simple and efficient repair techniques.

In a similar way, we have to point out the interest in airplane safety which arose after the Aloha accident [4,5] for civil aviation and after the Royal Australian Air Force Machi accident [5] for military aviation associated with the presence of cracks [6]. If the number of cracks is limited, and the crack or hole size is small compared to the damaged component, repairs are less expensive; otherwise, the component should be replaced [7].

Possible repairs include either replacement of a fastener or filling, or damage removal or patching. Conventionally, such defects were repaired by the use of doublers of like material where they were mechanically joined-fastened using rivets and bolts [8]. This approach has the advantage of compatibility of materials and simplicity of analysis. However, a major problem for the airplane structure is the development of small radial cracks below rivet heads and bolts, whereas the use of metallic sheets involves problems such as fatigue, galvanic corrosion, and difficulty of inspection after repair [9].

Bonded external patches, bonded scarf patches, and bolted external patches are possible options for patch repairs. The success of a bonding repair depends on the properties of the adhesive and the patch, and its affinity for the substrates. The quality of the bond also depends upon bonding procedure and surface preparation. The repair of metal structures by using composite materials is a technology that was first advocated in Australia in the early 1970s and later in the United States in the early 1980s [10].

Owing to several advantages, composite patching technology has quickly expanded to other countries, as well as other fields of science. Several experimental and numerical studies have been carried out on repairs [6–9]. These studies mainly focused on the effect of patch sizes (length and thickness) on the development of cracks, as well as on the fatigue behavior of repaired sheets. Unfortunately, very little work has been undertaken to study the aerodynamic effects of repairs devoted to the case of two-dimensional wings [11].

In this investigation, we are interested in the aerodynamic performance losses caused to a full aircraft (a light airplane model) by

Received 4 January 2008; revision received 6 June 2008; accepted for publication 21 June 2008.

*Lecturer, Fluid Mechanics Laboratory; s.djellal@gmail.com.
†Professor, Laboratoire d'Energétique, Mécanique et Matériaux; ouibraa@yahoo.fr.

the impact of battle damage on the wings, as well as the recovery of performances by mean of quick repairs. For this matter, we primarily investigate the aircraft model with undamaged and damaged wings by considering the variation of the hole diameter and its spanwise and chordwise positions. The subsequent objective of this investigation concerns recoveries which can be achieved with aircraft battle-damage repair (ABDR) patches through three aspects. In the first one, we consider the influence of different repair schemes (i.e., at intrados, extrados, and both). The influence of the patch shape (circular or square) is treated in the second one. The third one deals with the influence of patch thickness.

II. Experimental Program

A. Aircraft–Airfoil Models

The aircraft model presented in Fig. 1 is of solid construction and fully made of aluminum on a four-axis numerically controlled machine. The shape, dimensions, and profiles of the airplane parts were designed according to aerodynamic and structural constraints [12]. The wings are trapezoidal with a profile NACA 23018 at the root, NACA 23012 at the tip, with a taper ratio $\lambda = 0.5$, and without twist. The horizontal tail is rectangular with a profile NACA 0012 along the span, without dihedral. The same profile is used for the vertical tail. In accordance with the wind-tunnel size, the model built is 20 times smaller than full scale.

B. Damage Modeling

The damage range that can affect an airplane is wide. In this investigation, we consider that the damage is only located on the wings, which are, from the aerodynamic point of view, the most critical components of the airplane.

The most common type of damage used in simulations is the circular hole [13]. The study of other shapes reported by Mani and Render [14] has not shown noticeable differences. The influence of petaling that takes place around damage holes for a metal structure was not considered because the hole has the dominant effect [15]. Damage size can be expressed in terms of a percentage diameter d to the local chord length c. The range of damage sizes varies from 0.1 to 0.4 c [16] and, for our tests, three diameters, 0.2 , 0.3, and 0.4 c, have been considered. In Fig. 2, we have reported the hole details along with the wing dimensions, positions, and sizes of the damage. The original model was damaged by drilling the wing with a circular through hole normal to the chord.

According to the nature of the gunfire hits, the wing may be damaged at any point along the chord and the span. Three positions along the span are considered: tip region, fuselage or root region, and midway locations (Fig. 2).

Along the chord, four locations are generally used: leading edge, quarter of the chord, midchord, and trailing edge. We only considered wings damaged at the quarter- and the midchord, because they produced the greatest adverse influence on aerodynamic performance [2].

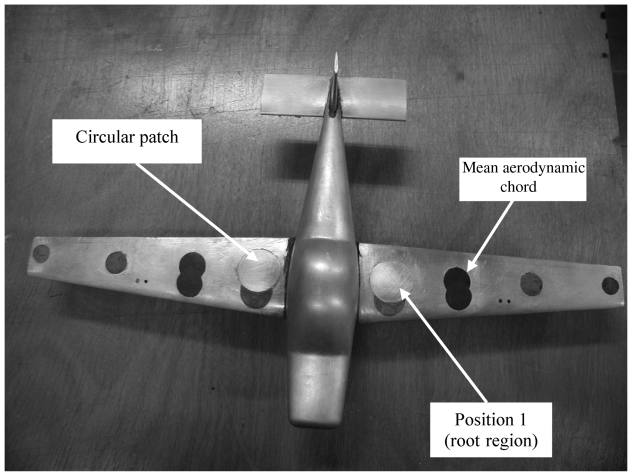

a) Circular patch

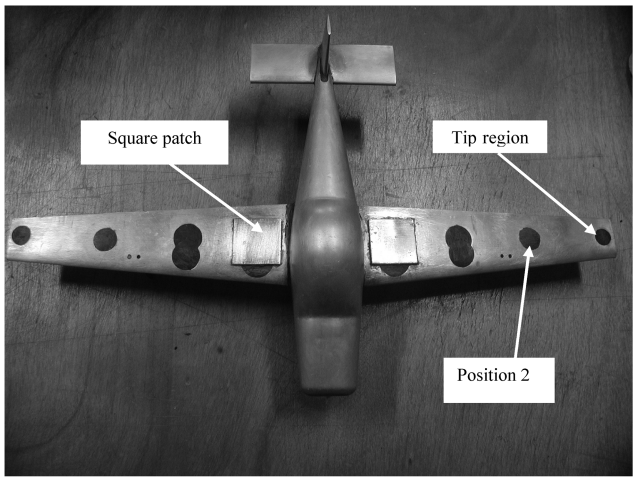

b) Square patch

Fig. 1 Aircraft model and repair patches.

C. Repair Modeling

The effect of repair on the aerodynamic performance of the model is investigated with a battle context in mind, where in some combat situations it may be appropriate to carry out rapid temporary repairs. Such repairs may consist of simple patches installed over the battle-damaged area to cover perforations in the skin.

In Fig. 1, we indicate the aircraft model with hole damages, as well as repair patches having different shapes applied at the extrados of the two wings. Repair patches are made of aluminum sheets. They were attached to the surface of the wing with 0.2 mm double-sided sticking tape. The square-edged patches used were oriented with their leading edge normal to the freestream direction. Table 1 gives the damage diameters subjected to repairs as well as the patch dimensions used for the two positions, as mentioned in Fig. 1, labeled position 1 and position 2. The circular patch diameter is taken equal to the square patch side such that the spanwise and chordwise extents are the same.

Based upon considerations of the United Kingdom's Royal Air Force ABDR and previous work [17], three repair situations or schemes are here investigated. For the first one, the patch is applied at the lower surface (intrados), whereas, for the second scheme, the patch is located at the upper surface (extrados), and, finally, for the third scheme (full scheme), two patches are applied on both surfaces lower and upper (both intrados and extrados).

III. Experimental Setup

A. Description

All the tests were conducted in the subsonic closed-return wind tunnel of the Fluid Mechanics Laboratory at Polytechnic School of Algiers (Fig. 3). This has a 0.6-m-diam test section and is capable of wind speed up to 48 m/s. The turbulence intensity of the incoming stream was found to be 1%, measured by using a TSI hot-wire anemometer.

The model was mounted via three struts to a three-component balance (Fig. 3). The incidence is manually adjusted over the range $[-20, +40$ deg]. The adjustment and the calibration of the balance are carried out according to well-defined steps. Efforts' measurements are carried out using three dynamometers FGP/FN 3148, whose electric signals are transmitted to the rack of measurement (Fig. 3).

The values of the aerodynamic efforts are directly linked to those read on the indicators of the rack by appropriate formulas. The data for each incidence angle are recorded after 20 s to ensure that the flow is well established.

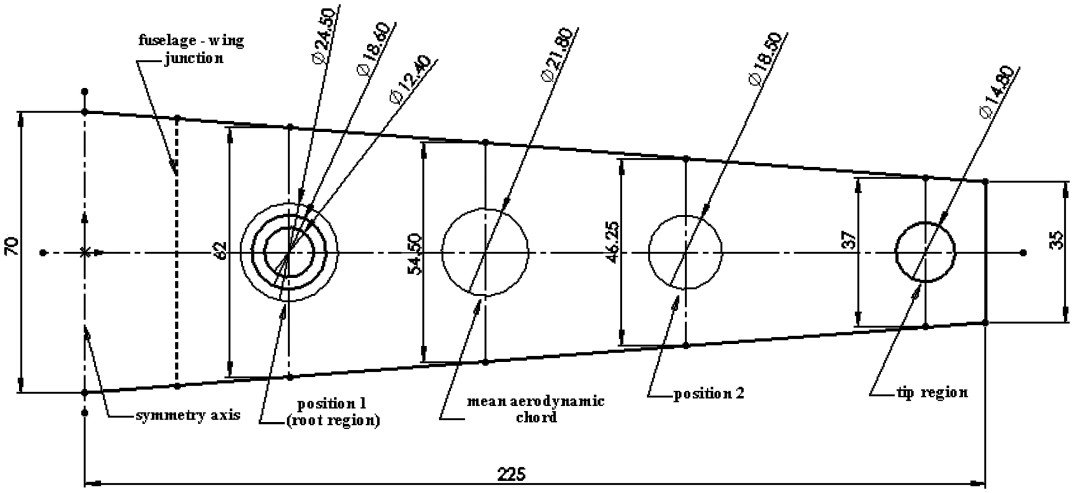

Fig. 2 Schematic of the wing with the major sizes in millimeters (hole damage diameters, local chords, span).

Because an open working section tunnel is being used, there is no need for tunnel corrections [18]. A smoke generator is used to visualize the jet issuing from the damage hole.

B. Flow Conditions

Two velocity values, 48 and 45 m/s, were used in the present investigation. For the study of the damage effect, we only used the limit value of 48 m/s allowed by the constructor. The corresponding Reynolds numbers, based on the wing mean chord, were 1.73×10^5 and 1.5×10^5, respectively, values which are below the critical Reynolds number.

C. Data Accuracy

The measurements carried out involve various equipment with corresponding accuracies given by the constructors. The measurements include the velocity, the aerodynamic effort, and the incidence angle; the variation of the temperature was negligible. Velocity measurements were carried out using a TSI hot-wire probe connected to a 16-bit National Instruments data acquisition system (NI 6052 E) with a sampling rate of 333 kS/s, so that the accuracy in velocity readings is on the order of 10^{-3} m/s.

As to the effort measurement, according to the constructor, the three dynamometers used have a nominal accuracy of 0.05% for a measurement range up to 10 daN. Regarding to the incidence angle α, it was manually adjusted with a maximum estimated error of 0.2 deg, which corresponds to an accuracy of 2.5% in the aerodynamic coefficients versus α curves. Assessment of repeatability indicated that uncertainties in the increments were ± 0.005 for lift and ± 0.002 for drag. Then, the estimated overall accuracy for lift and drag coefficients determined from measurements is finally ± 3 and $\pm 2.7\%$, respectively.

IV. Undamaged and Damaged States

A. Experimental Results

Preliminary tests are performed with the undamaged model to validate the experimental setup as well as to determine the aerodynamic characteristics of the model at the undamaged state.

Given the nature of the gunfire threat, the wing may be damaged on either one wing or both wings. For this purpose, we proceed first with tests for a single damaged wing and then for symmetrically damaged two wings (Figs. 4 and 5) with $d = 0.4c$ located at midchord and in the root region.

The comparison between these two situations indicates that C_L as well as C_D have similar trends with α, but we observe reduced values for the two-wings case with a factor of approximately 5%. It is worth mentioning that a single damage (only one wing) generates a roll moment due to lift-forces imbalance. This may be the source of a lateral instability. Moreover, this roll moment increases with incidence angle. A six-component balance would be required to estimate this roll moment. Therefore, for all the experiments conducted, we consider the case of symmetrically damaged two wings.

For the damaged model, as outlined earlier, the experiments have been carried out for different hole diameters (Figs. 6–8) and damage positions: along the span (Figs. 9 and 10) and along the chord (Figs. 11 and 12).

Table 1 Damage and repairs dimensions

	Position 1	Position 2
Damage diameter	24.5 mm	18.5 mm
Square patch side	35 mm	25 mm
Circular patch diameter	35 mm	25 mm

B. Effect of Hole Diameter

First, the damage hole affects the aerodynamic performances with an extent depending upon the size and the position of the hole. As a matter of fact, for a fixed diameter d and for all incidence angles α up to 14 deg, the lift coefficient C_L is decreased while the drag coefficient C_D is increased compared to the undamaged state (Figs. 6 and 7).

Second, the increase of d leads to an increase in the damage effect as shown by the decrease of C_L and the increase of C_D (Figs. 6 and 7). This is expected because a larger damage size allows a greater

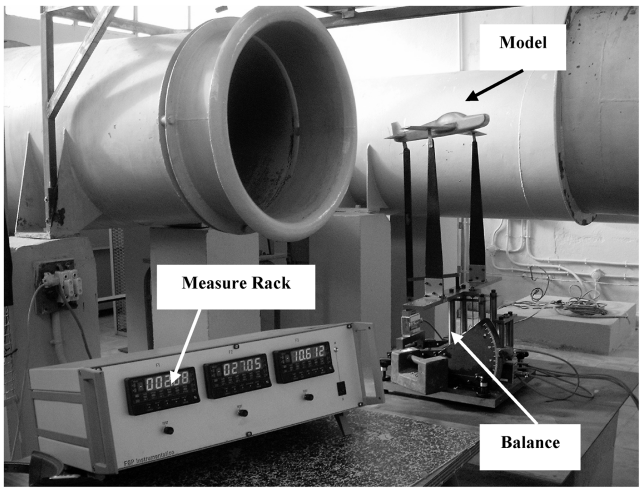

Fig. 3 Experimental setup.

through flow perturbing even more the pressure field distribution, as confirmed by the visualizations.

Besides the aerodynamic performance losses, the effect of the damage is also characterized by a stall angle shift toward higher values and a decrease of the maximum C_L. This shift can be attributed to the damage hole providing the upper surface with additional air flow from the lower surface, consequently disturbing the pressure field distribution. This disturbance considerably affects C_L and C_D.

C. Degradation of Fineness

For a general aerodynamic point of view, it is usually interesting to evaluate the whole performance (or the quality) of a wing through its fineness, $f = C_L/C_D$, which combines both C_L and C_D. In our case, such a representation will allow an evaluation of the extent of the damage on the aerodynamic situation of the wing when coupling both degradations of C_L and C_D. As a matter of fact, by combining the results of Figs. 6 and 7 in terms of fineness, Fig. 8 displays the extent of the damage hole size on the wings. Thus, it is easy to notice that f is drastically degraded by the damage diameter compared with the degradation of C_L (Fig. 6) and C_D (Fig. 7). For example, if we limit our comparison between only C_L and the fineness f, and consider the maximum of each one of them at undamaged and damaged states with $d = 0.4c$, we can notice (Figs. 6 and 8) a decrease of about 10% in the case of the increment of $(C_L)_{\max}$, whereas there is about a 30% decrease in the case of the increment of $(f)_{\max}$.

D. Effect of Damage Position Along the Span

For a fixed d, the position of the damage also affects C_L and C_D (Figs. 9 and 10), especially at large incidence angles in the case of C_L (Fig. 9) and significantly for both at the root region. Thus, the degradation of C_L and C_D increases from the tip to the root regions as can be expected.

E. Effect of Damage Position Along the Chord

The position of the damage along the chord also has a significant effect on the magnitudes of C_L and C_D (Figs. 11 and 12), more at the quarter-chord than at the midchord. Thus, for a fixed position on the span, the degradation of C_L and C_D decreases when the hole damage moves from the leading edge to the trailing edge. This damage effect is much more pronounced for C_L at larger values of α varying from 0 to 14 deg.

F. Data Analysis

1. Effect of the Damage Diameter

For a more detailed understanding of the influence of damage on both C_L and C_D, it is interesting to evaluate which is more affected by the damage hole. For this purpose, we consider the relative values of the aerodynamic losses, defined as follows:

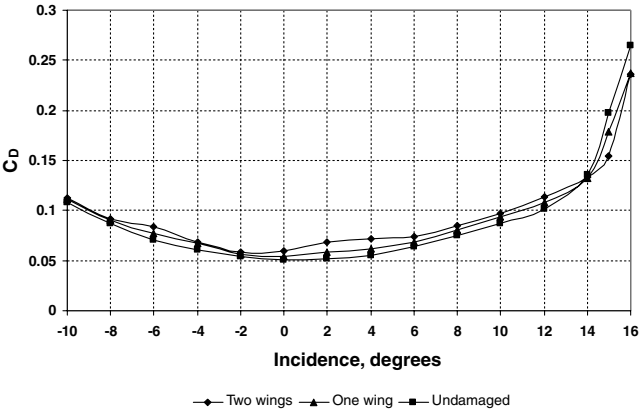

Fig. 5 Damage influence on C_D ($d = 0.4c$, midchord, root region).

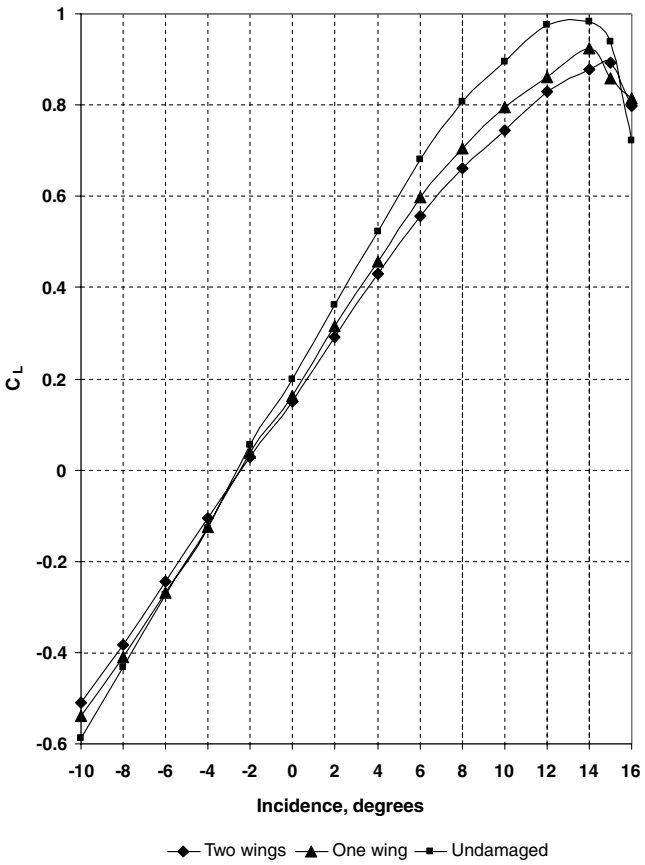

Fig. 4 Damage influence on C_L ($d = 0.4c$, midchord, root region).

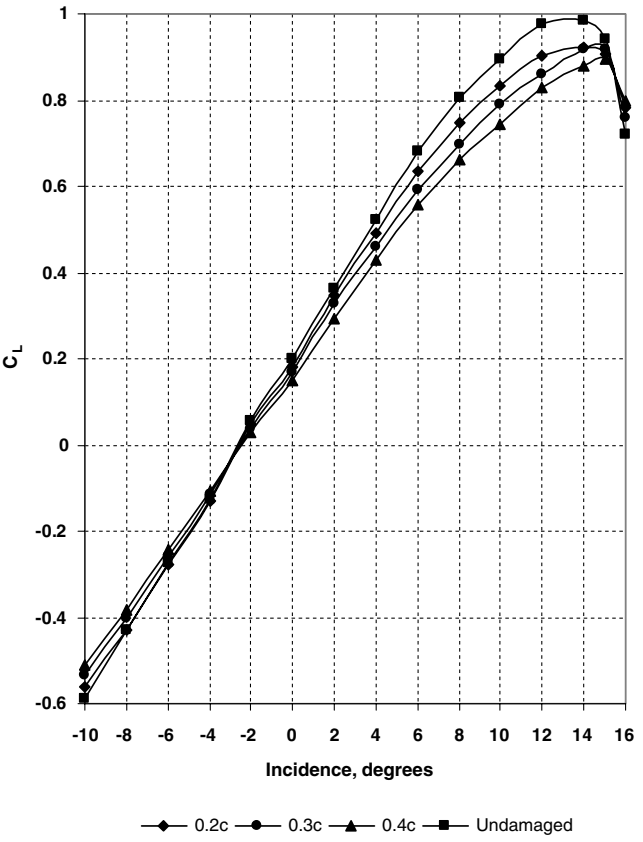

Fig. 6 Influence of damage diameter on lift coefficient (midchord, root region).

$$\overline{\Delta C_L}(\%) = \left(\frac{C_{L_{\text{damaged}}} - C_{L_{\text{undamaged}}}}{C_{L_{\text{undamaged}}}}\right)_{\alpha} \quad (1)$$

$$\overline{\Delta C_D}(\%) = \left(\frac{C_{D_{\text{damaged}}} - C_{D_{\text{undamaged}}}}{C_{D_{\text{undamaged}}}}\right)_{\alpha} \quad (2)$$

$$\overline{\Delta f}(\%) = \left(\frac{f_{\text{damaged}} - f_{\text{undamaged}}}{f_{\text{undamaged}}}\right)_{\alpha} \quad (3)$$

By using Eqs. (1) and (2), Figs. 6 and 7 lead to Figs. 13 and 14. Three interesting results can be found:

1) First, $\overline{\Delta C_L}$ and $\overline{\Delta C_D}$ increase with d from a maximum of 7% for C_L and 6% for C_D at $d = 0.2c$ to a maximum of 24% for C_L and 32% for C_D at $d = 0.4c$.

2) For all of the diameters, the relative degradation of C_L and C_D seems to remain constant (or slightly varying) for all α in the range of 0–14 deg, except for $d = 0.4c$ in the case of C_D, where instabilities are present owing to the "waviness" shown by the corresponding curve.

3) When comparing $\overline{\Delta C_L}$ and $\overline{\Delta C_D}$, Figs. 13 and 14 clearly indicate that, for all the hole diameters and for all values of α from 0 to 14 deg, the lift is more affected than the drag.

In the case of the fineness representation, Eq. (3), together with the results of Fig. 8, lead to Fig. 15. It is clear from Fig. 15, compared with Figs. 13 and 14, that, with the fineness representation, we can better and fully appreciate the damage extent result of gathered damages occurring to both C_L and C_D, as shown, for example, for the largest hole ($0.4c$) and for α varying from 6 to 14 deg, by the loss variations of $\overline{\Delta C_L}$ (from 18 to 11%), of $\overline{\Delta C_D}$ (from 15 to 0%), and of $\overline{\Delta f}$ (from 30 to 10%). This last variation is practically the sum of the first two.

2. *Effect of Damage Position Along the Span*

From Figs. 8 and 9, with Eqs. (1) and (2), we obtain Figs. 16 and 17, where it clearly appears that the magnitude of the damage effect is sensitive to its position along the span. In the case of the lift (Fig. 16), the degradation $\overline{\Delta C_L}$ increases as the position moves from the tip toward the root region. For example, at 2 deg, $\overline{\Delta C_L}$ varies from 2% at the tip region to 20% at the root region; whereas, for a fixed position, $\overline{\Delta C_L}$ remains almost constant for incidences between 0 and 14 deg.

Like $\overline{\Delta C_L}$, $\overline{\Delta C_D}$ increases from the tip to the root region. Although remaining constant (around 2%) at the tip region for all values of α, in the case of the mean aerodynamic chord and the root region, $\overline{\Delta C_D}$ decreases from values as large as 25% with α increasing from 0 to 14 deg (Fig. 17).

3. *Effect of Damage Position Along the Chord*

From Figs. 10 and 11, with Eqs. (1) and (2), we obtain Figs. 18 and 19, where it can be seen that the magnitude of the damage effect on the lift and as well as the drag is also sensitive to its position along the chord. This effect is more significant at the quarter-chord than at the midchord. In the case of lift (Fig. 18), $\overline{\Delta C_L}$ is drastically enhanced when the hole is located at the quarter-chord, reaching values as large as 40% and decreasing down to 20% at the midchord. Moreover, as along the span case (Fig. 16), it is also interesting to observe that $\overline{\Delta C_L}$ also remains almost constant for all α, from 2 to 10 deg, or slightly increases from 0 to 14 deg; the two curves (quarter- and midchord) are practically parallel.

In the case of $\overline{\Delta C_D}$ (Fig. 19), although we have a similar effect of the hole position along the span, the two corresponding curves exhibit a quite different trend compared with those of $\overline{\Delta C_L}$. For the midchord, $\overline{\Delta C_D}$ increases first to reach a maximum of 32% at 2 deg and then decreases significantly down to 0% for α increasing up to 14 deg. In the case of the quarter-chord, $\overline{\Delta C_D}$ increases with increasing α to reach a maximum of 40% for $\alpha = 12$ deg and then abruptly decreases down to 0% for α exceeding 14 deg.

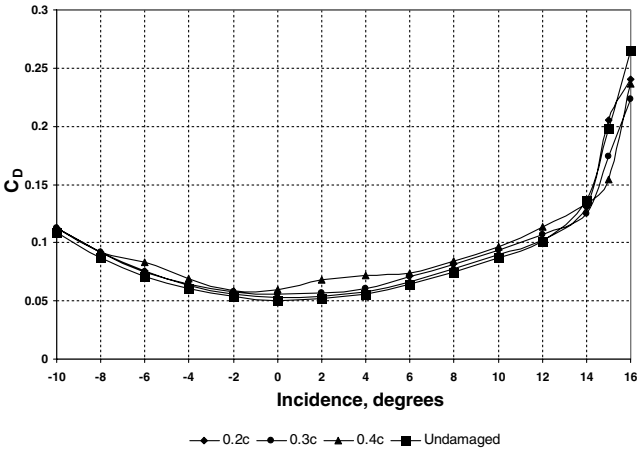

Fig. 7 Influence of damage diameter on drag coefficient (midchord, root region).

4. *Impact of Hole Size on C_L and C_D*

To analyze the impact of the hole dimensions on the degradation of C_L and C_D, we consider the behavior of the increments of C_L and C_D by unit relative hole surface. More precisely, these increments are normalized to the relative surface of the damage hole ΔS, as follows, where $\Delta S = A/S$, A is the hole surface at the local chord, and S the wing surface:

$$\frac{\Delta C_L}{\Delta S} = \frac{C_{L_{\text{damaged}}} - C_{L_{\text{undamaged}}}}{\Delta S} \quad (4)$$

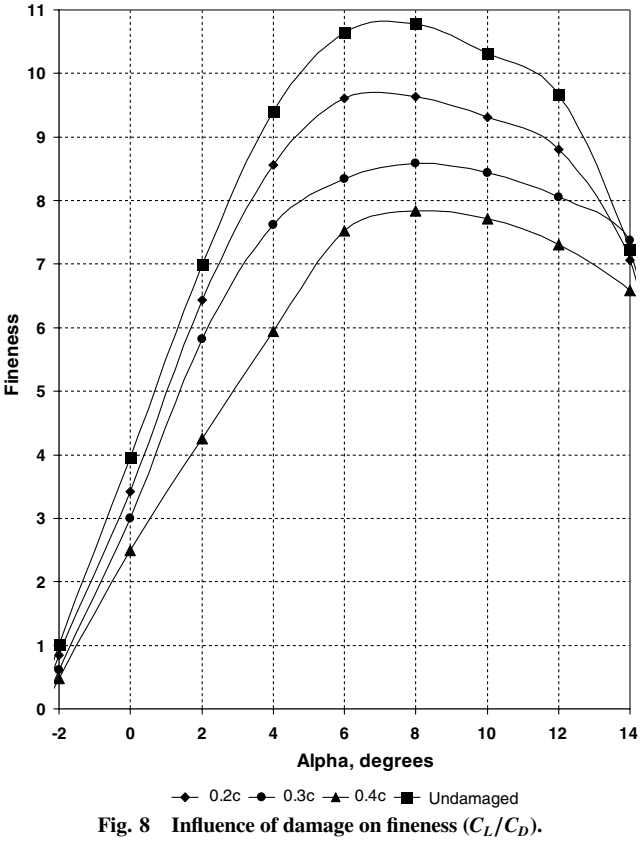

Fig. 8 Influence of damage on fineness (C_L/C_D).

$$\frac{\Delta C_D}{\Delta S} = \frac{C_{D_{\text{damaged}}} - C_{D_{\text{undamaged}}}}{\Delta S} \tag{5}$$

Figures 20 and 21, obtained from Figs. 6 and 7 with Eqs. (4) and (5), display two quite interesting results. In the case of C_L, Fig. 20 indicates that the three curves $\Delta C_L/\Delta S$ versus α associated with the three hole diameters remain distinct for $4 \leq \alpha \leq 16$ deg; whereas, in the case of $\Delta c_D/\Delta S$, the three curves corresponding to the three hole diameters definitely collapsed in one curve for all α varying from 4 to 16 deg. These interesting results suggest that, in the case of the lift, it is mainly the pressure distribution from the hole which leads for each incidence angle position to a new (then degradation) of C_L, but not the wing surface reduction; whereas, in the case of the drag, the increments of C_D are proportional to the surface of the hole damage at the local chord. The increase of C_D arises then from the thrust of the jet issuing from the area of the hole at given α.

5. *Flow Visualizations*

The different aforementioned damage effects on the degradation of the lift and the drag are undoubtedly a consequence of the disturbed flow configuration at the damage hole position. Visualizations performed at the damage location (Fig. 22) indeed suggest the disturbance of the flowfield depending on the magnitude of the jet issued from the hole. The jet penetrating by the hole takes two different forms. The first form is a "weak jet" (Fig. 22a), which forms an attached wake for small incidence angles (less than 4 deg). In this case, the jet exits only through the rear portion of the damage hole. The second form is a "strong-jet" (Fig. 22b), which forms a separated wake for higher attack angles (greater than 5 deg); the jet completely fills the hole and the width of the jet wake becomes significantly more important than the previous case. The terminology of weak and strong jets is adopted from investigations into "jets in crossflow" [2,19].

Increasing the hole diameter changes the jet shape from weak jet to strong jet. This is accompanied by an increase of the performance

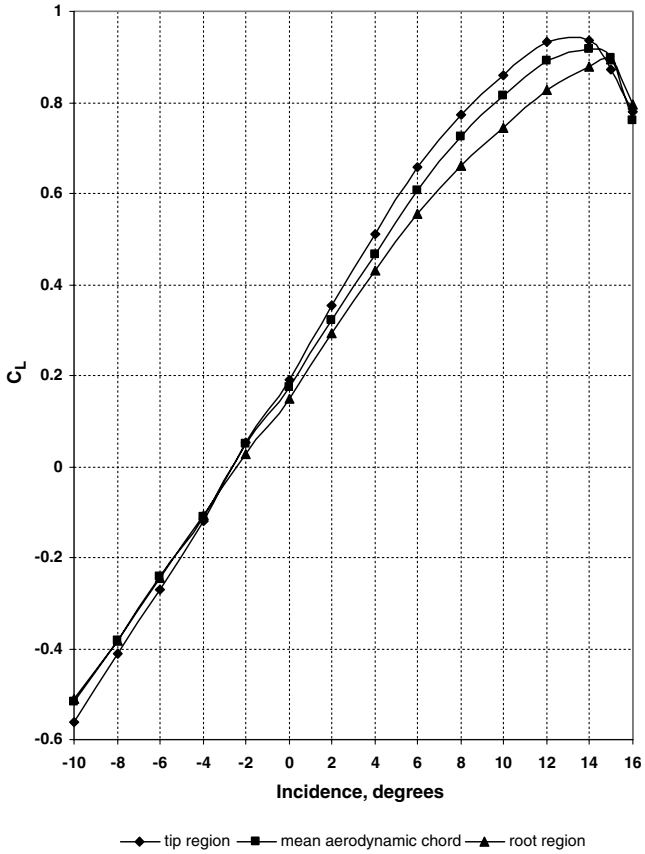

Fig. 9 Spanwise influence of damage on lift coefficient ($d = 0.4c$, midchord).

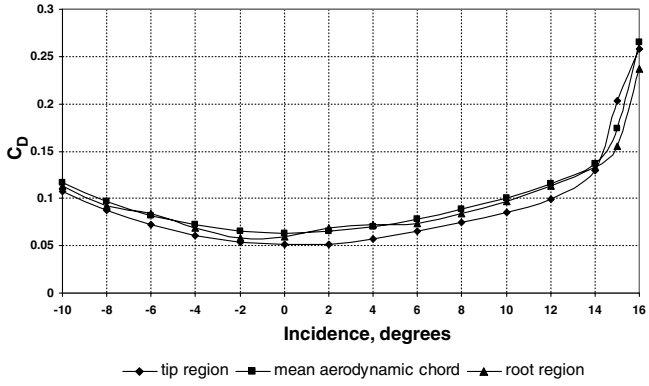

Fig. 10 Spanwise influence of damage on drag coefficient ($d = 0.4c$, midchord).

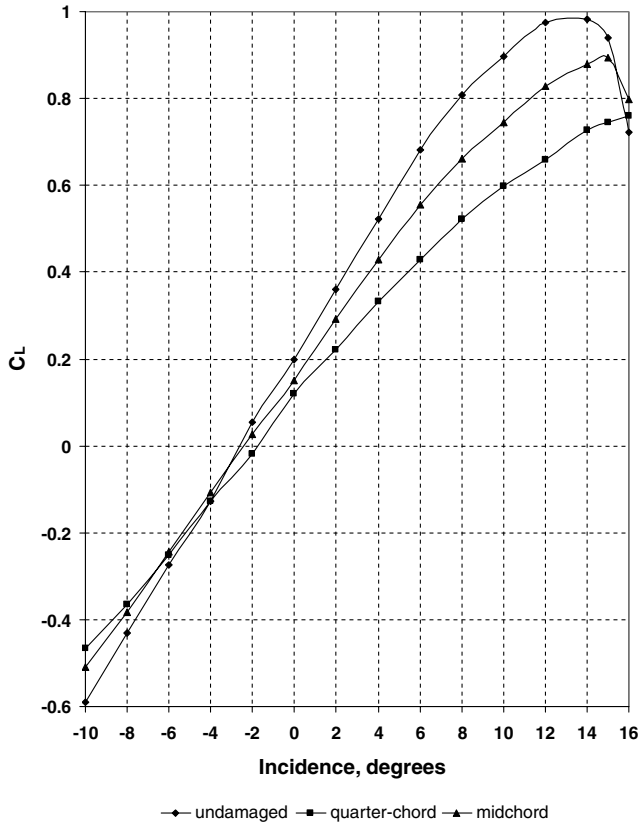

Fig. 11 Chordwise influence of damage on lift coefficient ($d = 0.4c$, root region).

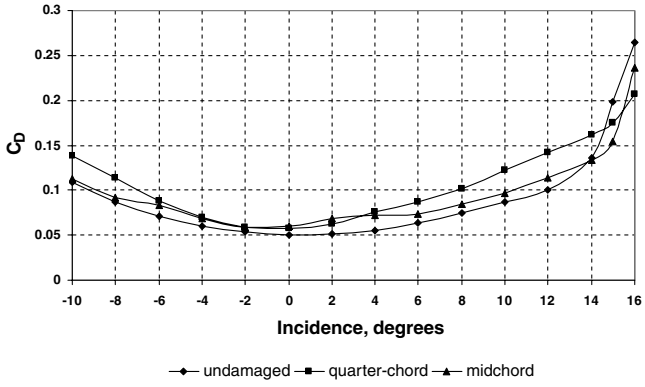

Fig. 12 Chordwise influence of damage on drag coefficient ($d = 0.4c$, root region).

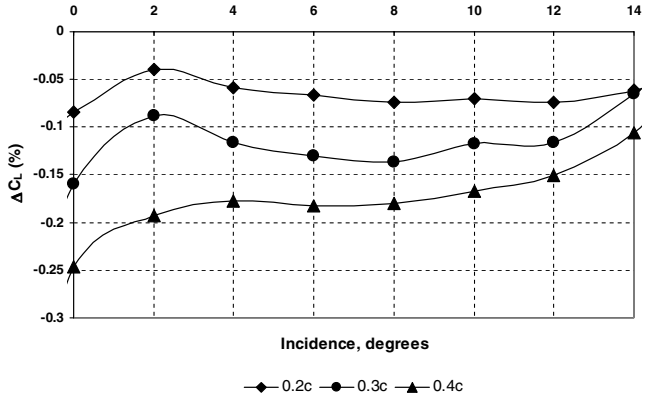

Fig. 13 Rate of lift coefficient loss for different hole diameters (hole position: midchord, root region).

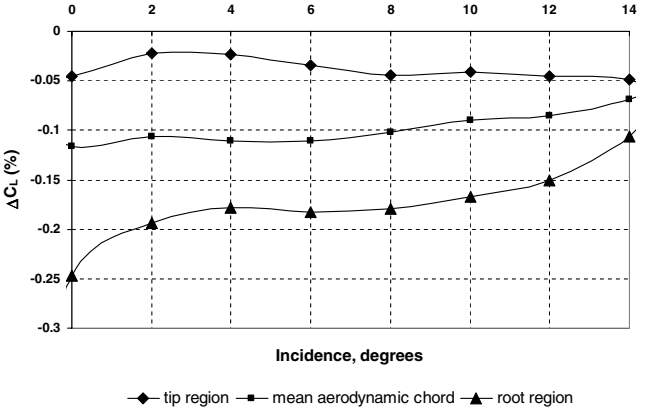

Fig. 16 Rate of lift coefficient loss along the span ($d = 0.4c$, midchord).

losses. The shape of the penetrating jet also varies with the angle of incidence. At the angle of zero lift corresponding to $\alpha_{ZL} = -2.5$ deg, there are no losses. Indeed, for this angle, there is no through flow. In our experiments, we have confirmed the existence of through flow for 0 deg angle. Above this value, and for all the attack angle range corresponding to positive lift, the direction of the flow is bottom to top. By generating a negative lift, the direction of the flow is reversed.

V. Repaired States

For this part, we consider two damage holes, each one having a diameter of 40% of the local chord c as described in Table 1. These holes are both centered at the midchord and are located at two different spanwise wing positions, labeled position 1 and 2, respectively, in Fig. 2.

Referring to the previous results obtained in the case of the damaged state, this value of the hole diameter as well as position 1 were selected to have the maximum aerodynamic performance loss due to the damage, and, therefore, we can expect a larger improvement upon repair. Position 2 is selected for comparison purposes.

The influences of repairs on the aerodynamic performances are considered through three different repair parameters: the scheme (lower, upper, or full repair) and the shape (circular or square), as well as the thickness of the patch.

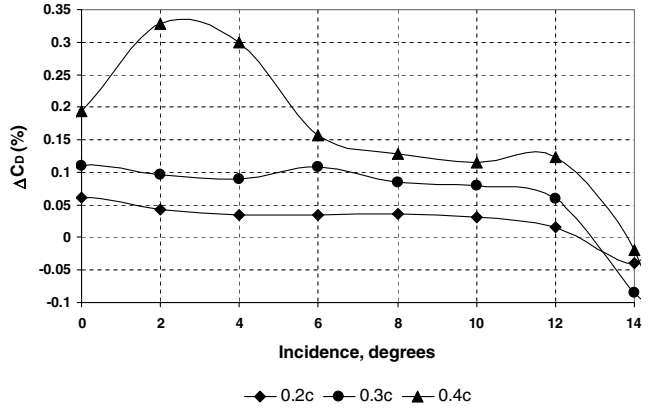

Fig. 14 Rate of drag coefficient increase for different hole diameters (hole position: midchord, root region).

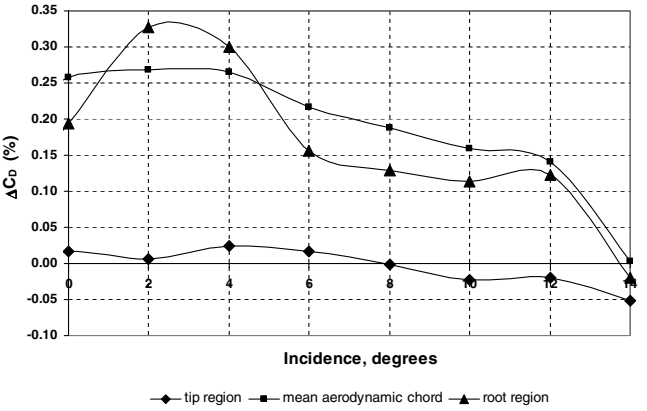

Fig. 17 Rate of drag coefficient increase along the span ($d = 0.4c$, midchord).

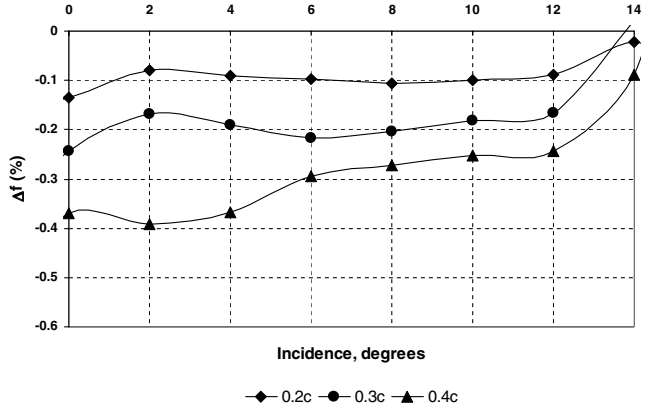

Fig. 15 Rate of fineness loss for different hole diameters (hole position: midchord, root region).

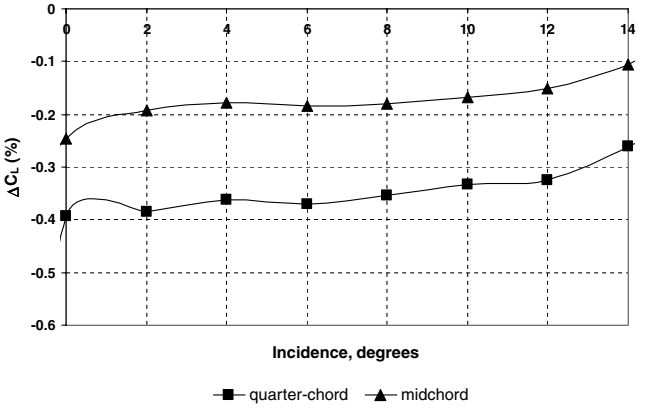

Fig. 18 Rate of lift coefficient loss along the chord ($d = 0.4c$, root region).

A. Experimental Results

1. Influence of Repair Schemes

Three repair configurations were studied for each damage scenario, namely, full, upper, and lower repairs. The thickness of the circular patch used here was 0.2 mm. Figures 23 and 24 show that, for α varying from 0 to 14 deg, all repair schemes provided improvements to the C_L and C_D values located between the undamaged and damaged ones. At this stage, the best scheme for improvement does not clearly appear; this point will be further considered at data analysis.

In regard to the fineness, Fig. 25 shows that, of course, all repair schemes provide improvements to the fineness values. The full repair, as expected, provides the best improvement over most of the incidence interval, whereas the upper and lower repair curves are practically the same.

For low incidence ($\alpha < 6$ deg), the fineness values are closer to those of the undamaged state, whereas, above the angle of maximum fineness ($\alpha > 8$ deg), the improvement decreases up to $\alpha = 14$ deg (stall angle). It must be outlined, as also shown in Fig. 25, that all repairs restore the undamaged angle of maximum fineness value (8 deg).

2. Influence of Repair Shape

We consider a full scheme repair for two shapes of patch, circular and square, having a thickness of 0.6 mm. Figure 26 shows that the circular patch gives better improvements than the square patch for C_L, whereas improvement is less pronounced in the case of C_D (Fig. 27), particularly for $\alpha > 6$ deg.

In the case of the fineness, the effect of the repair shape is quite a bit more apparent; Fig. 28 clearly shows that the circular patch gives better performance than the square patch. The fineness increment for circular patches is about twice that of square patches over the majority of the incidence angles.

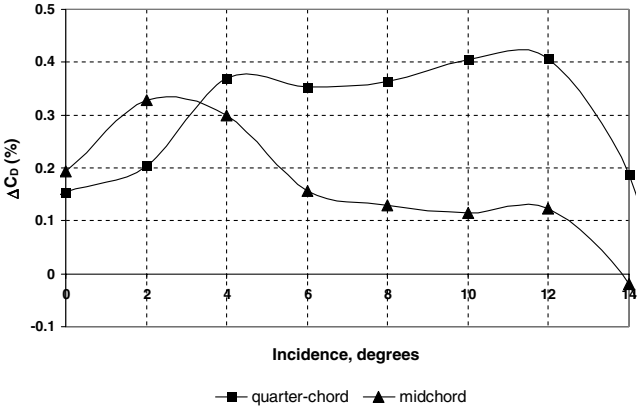

Fig. 19 Rate of drag coefficient increase along the chord ($d = 0.4c$, root region).

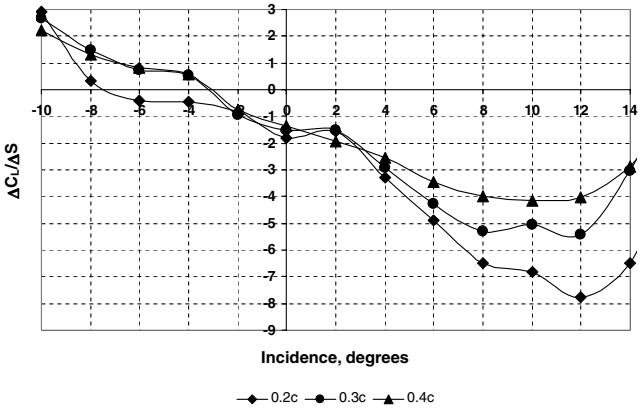

Fig. 20 Normalized increment of lift coefficient (hole position: midchord, root region).

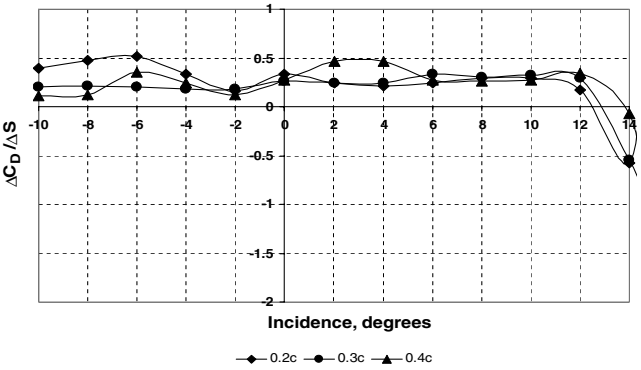

Fig. 21 Normalized increment of drag coefficient (hole position: midchord, root region).

3. Influence of Repair Thickness

Measurements were carried out for four circular and square patches, of thickness $e = 0.2$, 0.6, 1, and 1.4 mm, corresponding to nondimensional relative thickness (to the local chord c) of values $\bar{e}_1 = 0.3\%$, $\bar{e}_2 = 1\%$, $\bar{e}_3 = 1.6\%$ and $\bar{e}_4 = 2.3\%$. We only present here the full scheme results.

Figures 29–32 reveal that the extent of the patch thickness influence is different from one shape to another, as well as from C_L to C_D. As a matter of fact, in the case of C_L and with the circular patch (Fig. 29), the increase of the thickness $\bar{e}$ involves a decrease of the improvements of C_L for all incidence angles and, for the largest value $\bar{e}_4$, the values of C_L are below the damaged ones. These observations

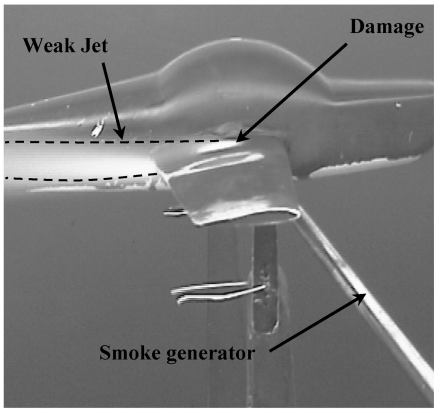

a) $\alpha = 4°$

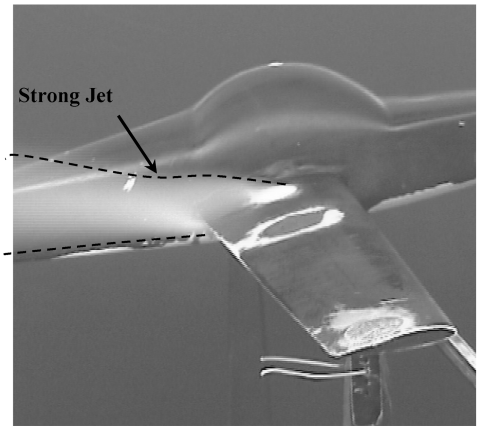

b) $\alpha = 6°$

Fig. 22 Smoke visualization for damaged aircraft's model.

are more pronounced in the case of the square patch (Fig. 30), where C_L has values below the damaged ones for the largest thicknesses $\bar{e}_3$ and $\bar{e}_4$.

In the case of the drag, and for all the patch thicknesses and shapes, the values of C_D are always above the damaged ones (Figs. 31 and 32). For the circular patch, the difference between each thickness clearly appears. The largest thickness $\bar{e}_4$ exhibits improvements less than the others, whereas the smallest values $\bar{e}_2$ and $\bar{e}_1$ involve values of C_D close to those of the undamaged state.

For the square patch (Fig. 32), the effect of $\bar{e}$ is even more evident. Clearly, the improvements of C_D decrease when $\bar{e}$ increases. The obtained values are between the damaged and the undamaged ones, close or equal to the last ones for the smallest value $\bar{e}_4$, depending on the value of α.

Of course, in the case of the fineness for the circular patches, Fig. 33 clearly shows improvements of the damaged fineness for all thicknesses and for all incidence angles below 14 deg; this improvement decreases with the increase of the thickness. However, for α larger than 14 deg, all thicknesses lead to fineness values smaller that those of the unrepaired wing.

For the square patch, Fig. 34 results are quite a bit less interesting. Comparable improvements to those of the circular patch for all α below 14 deg are obtained only for the smallest thickness ($\bar{e}_1 = 0.3\%$) while limited to $\alpha \leq 10$ deg for the next smallest $\bar{e}$ ($\bar{e}_2 = 1\%$). The increase of $\bar{e}$ to $\bar{e}_3$ and $\bar{e}_4$ leads then to a decrease in the fineness values below those of the damaged wing as α increases from $\alpha \leq 8$ deg. This results from the effect of large value of thickness $\bar{e}$ on the lift, as previously outlined.

B. Data Analysis

For a better perception of the effects of the different repairs described earlier and a better evaluation of these effects, the corresponding results given previously are transcribed first in terms of increments of losses as well as of gains (or recoveries) of C_L and C_D via repairs and, second, in terms of percentage of losses and recoveries allowed for C_L, C_D, and f by the different kinds of the indicated repairs. The increments of ΔC_L and ΔC_D are defined from the undamaged state as follows:

For the damaged state or loss

$$\Delta C_{L_{\text{damaged}}} = C_{L_{\text{damaged}}} - C_{L_{\text{undamaged}}} \tag{6}$$

$$\Delta C_{D_{\text{damaged}}} = C_{D_{\text{damaged}}} - C_{D_{\text{undamaged}}} \tag{7}$$

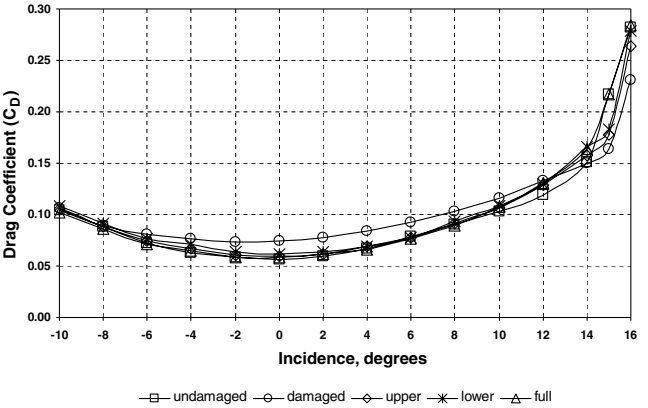

Fig. 24 Influence of repair schemes on C_D (position 1, $d = 0.4c$, $e = 0.6$ mm).

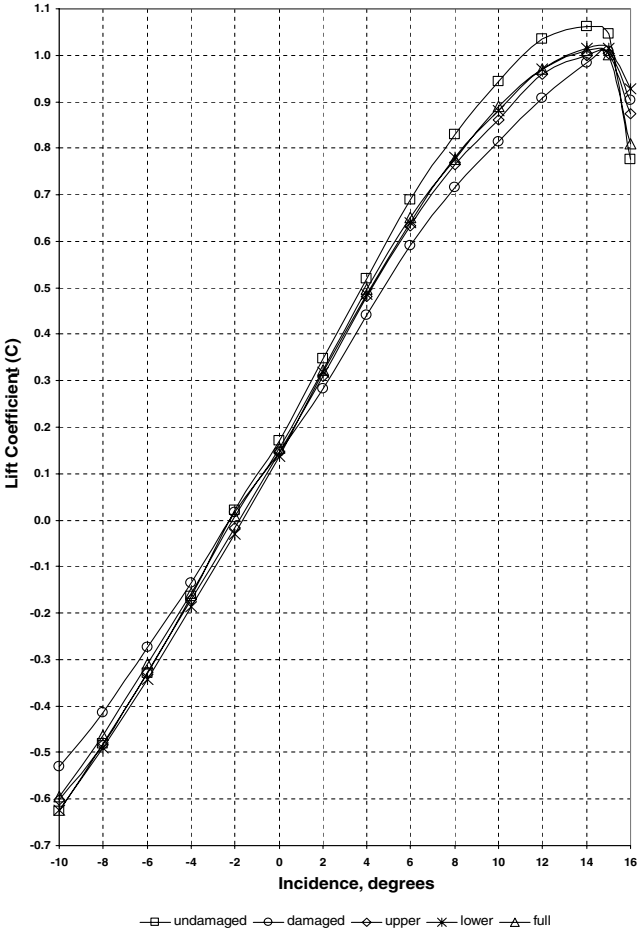

Fig. 23 Influence of repair schemes on C_L (position 1, $d = 0.4c$, $e = 0.6$ mm).

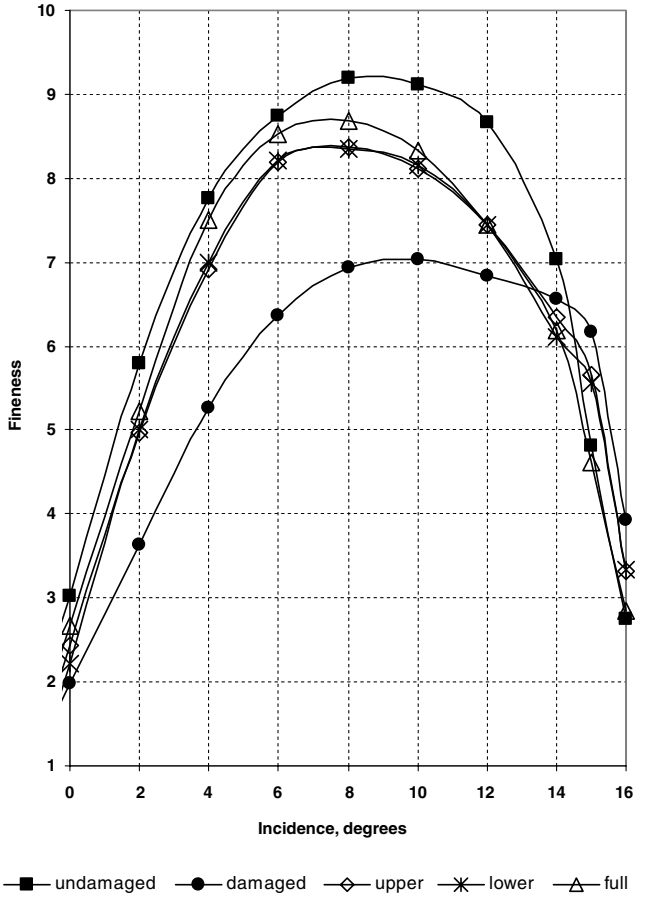

Fig. 25 Influence of repair schemes on the fineness (position 1, $d = 0.4c$, $e = 0.6$ mm).

For the repaired states or recoveries

$$\Delta C_{L_{\text{repair scheme}}} = C_{L_{\text{repair scheme}}} - C_{L_{\text{undamaged}}} \tag{8}$$

$$\Delta C_{D_{\text{repair scheme}}} = C_{D_{\text{repair scheme}}} - C_{D_{\text{undamaged}}} \tag{9}$$

For lost and recovered performances

$$\overline{\Delta C_{L_{\text{loss}}}}(\%) = \left(\frac{C_{L_{\text{damaged}}} - C_{L_{\text{undamaged}}}}{C_{L_{\text{undamaged}}}}\right)_{\alpha,\text{damaged situation}} \tag{10}$$

$$\overline{\Delta C_{L_{\text{repair scheme}}}}(\%) = \left(\frac{C_{L_{\text{repair scheme}}} - C_{L_{\text{undamaged}}}}{C_{L_{\text{undamaged}}}}\right)_{\alpha,\text{damaged situation}} \tag{11}$$

We define, as well, $\overline{\Delta C_{D_{\text{loss}}}}(\%)$, $\overline{\Delta C_{D_{\text{repair scheme}}}}(\%)$, $\overline{\Delta f_{\text{loss}}}(\%)$, and $\overline{\Delta f_{\text{repair scheme}}}(\%)$.

C. Effect of the Repair Scheme

1. Increments of C_L and C_D

First of all, in terms of increments, when using the relations (6) and (8) together with the results of Fig. 23 for C_L, we clearly notice in Fig. 35 that, compared with the damaged state, there are indeed significant improvements in C_L for all the repair schemes. The gained increments of C_L of each repair scheme have values close to each other. The full scheme appears to involve the best improvements whereas the inverse applies for the upper one.

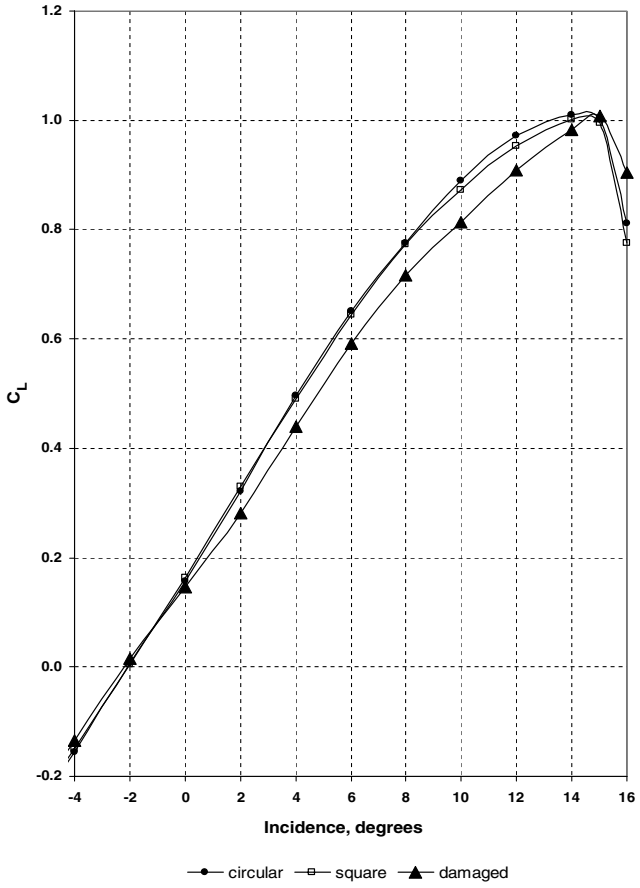

Fig. 26 Influence of the repair shape on C_L (position 1, $d = 0.4c$, $e = 0.6$ mm).

In the same way, for the increments ΔC_D, obtained from Fig. 24 with Eqs. (7) and (9), significant improvements are perceptible (Fig. 36), and they are the best in the case of the full repair, as noticed for C_L.

Such an observation on the predominance of the full scheme can be explained. As a matter of fact, in the case of lower and upper schemes, repairing only one surface does not completely restore the geometry of the wing surfaces, so that the upper or lower remaining hole acts as a circular cavity, inducing a pressure drag increment. The flow structure around the cavities is a complex study [20] and is beyond the scope of this work.

2. Rate of Loss and Recoveries for C_L, C_D, and f

In terms of rate of loss and recoveries, when using results of Figs. 23–25 with Eqs. (10) and (11) and so on, it clearly appears in Figs. 37 and 38 that the full repair benefits more for C_D than for C_L, leading to values of recovered C_D close to those of the undamaged state. For example, in Fig. 38 at $\alpha = 0$ deg, the value of C_D has degraded down to 30% for the damaged state (compared to the

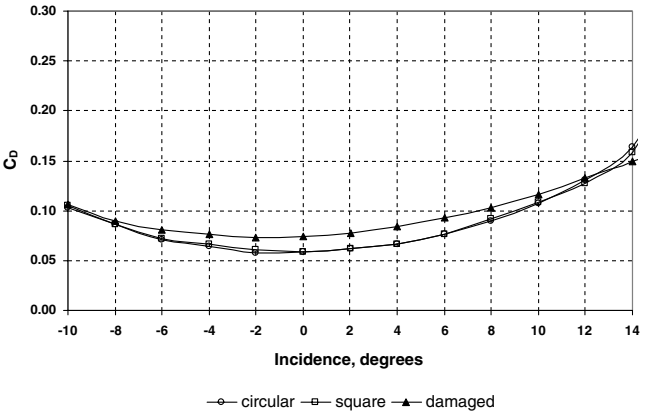

Fig. 27 Influence of the repair shape on C_D (position 1, $d = 0.4c$, $e = 0.6$ mm).

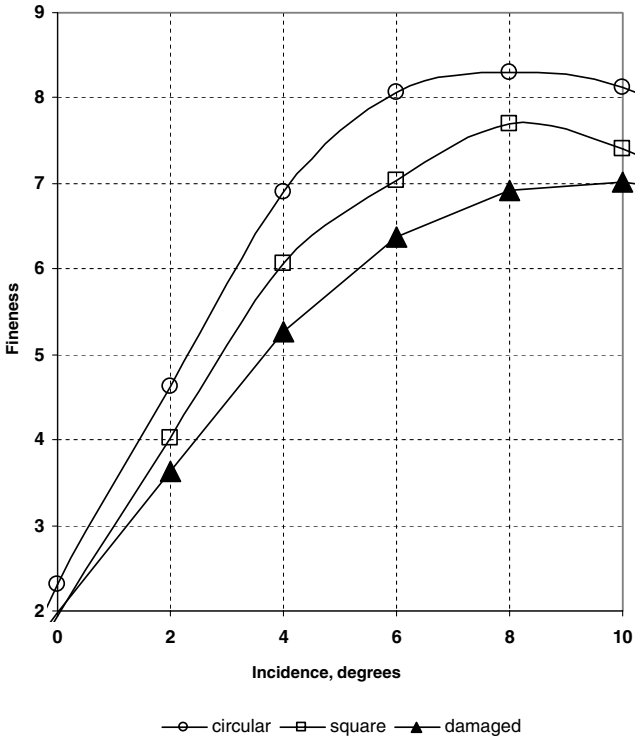

Fig. 28 Influence of repair shape on the fineness (position 1, $d = 0.4c$, $e = 0.6$ mm).

undamaged state); whereas, we notice a full recovery of C_D with the full repair. This full recovery is still observed for larger values of α. For instance, at $\alpha = 8$ deg, there is the full recovery of the 15% initially lost at the damaged state. Whereas, in the case of C_L, although as previously outlined the full repair gives better recoveries, the recovery is never complete and the gain is then less important than for C_D. For $\alpha = 0$ deg, the gain is equal to 5% ($\overline{\Delta C_{L_{\text{loss}}}} = 15\%$, $\overline{\Delta C_{L_{\text{full scheme}}}} = 10\%$) and at $\alpha = 12$ deg this gain is still around 5% ($\overline{\Delta C_{L_{\text{loss}}}} = 12\%$, $\overline{\Delta C_{L_{\text{full scheme}}}} = 5.7\%$).

Lastly, in the case of the fineness, Fig. 39, as a consequence of Figs. 37 and 38 or Fig. 28 with the corresponding relations to Eqs. (10) and (11), clearly indicates that the fineness $\Delta f_{\text{loss/damage}}$ varies from 34.7% at 0 deg to 37.2% at 2 deg and then decreases down to 21% at 12 deg to reach a value as small as 7% at 14 deg. All the repair schemes lead to improvement of the fineness compared to $\Delta f_{\text{loss/damage}}$. The full repair offers the best recovery; at 0 deg the gain from the damaged state is about 25% and, at 6 deg, where the fineness value approaches the undamaged one, the gain is still about 25%. The upper and lower repairs display the same values for the whole range of incidence. Their gains in recovery are smaller than those of the full repair.

3. *Effect of Repair Shape*

We consider a full scheme repair patch having a thickness of 0.6 mm for two shapes (circular and square). For this section and the next, owing to the results of the previous section, we definitely consider the relative loss and recoveries of C_L and C_D, and analyze the impact of the repair shape on these aerodynamic coefficients.

Figures 26 and 28, together with Eqs. (10) and (11), lead to Figs. 40–42 describing the relative loss and the recoveries of each of these coefficients. Thus, beginning with C_L, we notice clearly in Fig. 40 that the circular patch offers better improvements than the square one, for which the recovered values practically match those of the damaged wings. For the circular patch, the gain varies from 3% at 2 deg to 9% at 10 deg, decreasing to 4% at 12 deg.

In the case of C_D (Fig. 41), the improvements are quite significant compared with C_L for both circular and square shapes. The recoveries are largest with the circular patch provided that α is less than 8 deg. The gain reaches 30% at 0 deg (full recovery) to down to 4% at 12 deg.

For the fineness, Fig. 42 is clearly explicit. There are, of course, the significant improvements involved by the two patch shapes, although the circular patch offers the best improvements. It is interesting to note that these improvements have the same trend when α varies from 0 to 12 deg, and that the values corresponding to the improvements of the square patch are halfway between the damaged state and the circular patch repair. With the circular patch, the gain begins at 10% for 0 deg, to reach 21% at 4 deg, and decreases while α increases.

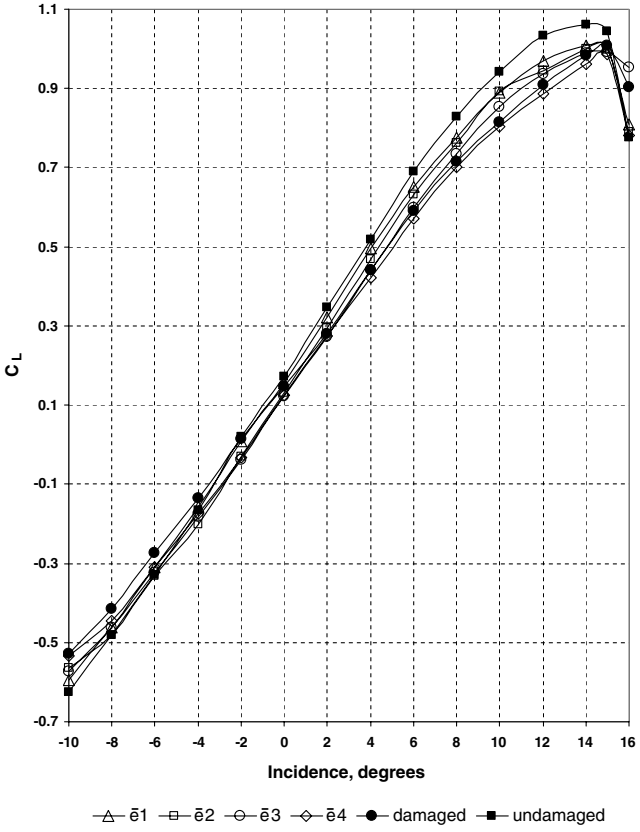

Fig. 29 Influence of repair thickness on C_L (circular patch, full scheme).

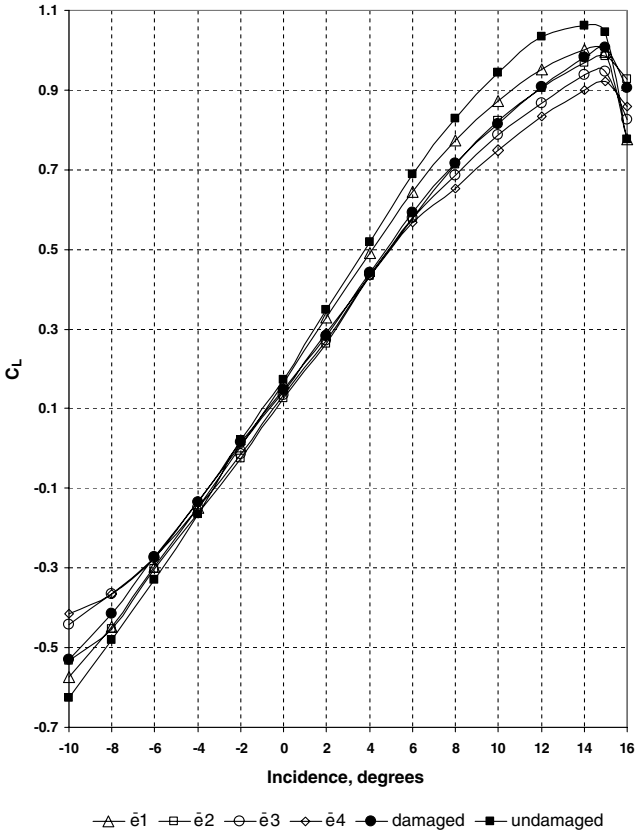

Fig. 30 Influence of repair thickness on C_L (square patch, full scheme).

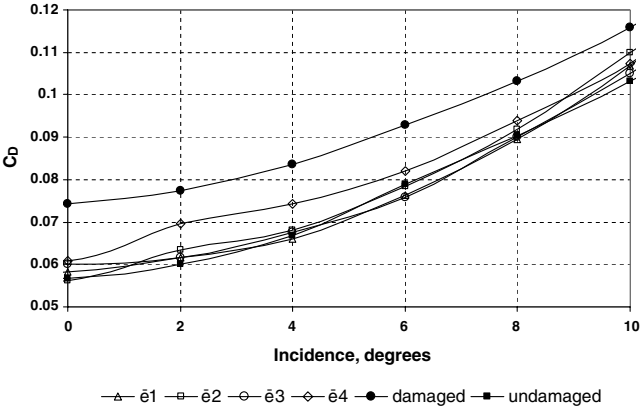

Fig. 31 Influence of repair thickness on C_D (circular patch, full scheme).

4. Effect of Repair Thickness

For C_L, as a result of Figs. 29 and 30 together with Eqs. (10) and (11), Figs. 43 and 44 exhibit interesting results when compared to each other. Thus, in the case of the circular patch (Fig. 43), the discrepancies between the improvements corresponding to the four thicknesses are not so pronounced as for the square shape. Of course, the best improvement is obtained for the smallest thickness $\bar{e}_1$ where the gain is around 5% at 0 deg, reaching 10% at 4 deg, decreasing to 2% at 14 deg. The recoveries decrease with the increase of the thickness and, for the largest one $\bar{e}_4$, there is no longer recovery for all α; rather, the values of C_L are below those of the damaged state, an additional decrease of about 2–3%.

Finally, even with the smallest thickness $\bar{e}_1$, the obtained recovery is not complete compared with the undamaged state. There is a recovery of 95% of the original (undamaged) lift with a thin enough circular patch.

On the other hand, for the square patch (Fig. 44), the discrepancies between the improvements are pronounced. We first notice that the improvement holds practically only for the smallest thickness $\bar{e}_1$; below 4 deg from the damaged state, the gain is on the order of 10% and decreases down to 3% at 14 deg. With the second thickness $\bar{e}_2$, we obtain no improvements and the values of C_L are close to those of the damaged state. For $\bar{e} > \bar{e}_2$ and for all α, especially exceeding 6 deg, there is rather more degradation of C_L from the damaged state. This degradation increases with the increase of $\bar{e}$. Compared to the damaged and the undamaged states, this degradation may reach $\bar{e}_3$ values as large as 4 and 16%, respectively, and for $\bar{e}_4$, 7 and 20%, respectively. This means that the lift can degrade more than the damaged state, when repairing at full scheme with square patches that are too thick. This leads to an interesting observation: adding just two square patches on the intrados and extrados of a wing, even undamaged, will provoke a decrease of the lift if the patches are thick enough. In fact, with the thicknesses of such patches, there is the ability to locally disturb the flowfield, then inducing a perturbation of the pressure distribution along the intrados and extrados favorable to reduce the lift.

Proceeding in the same way as for C_L, Figs. 31 and 32 together with the corresponding Eqs. (10) and (11), lead to the Figs. 45 and 46 for C_D. First of all, we notice that all the patch thicknesses involve improvements with all the shapes (contrary to C_L) unless α is equal to

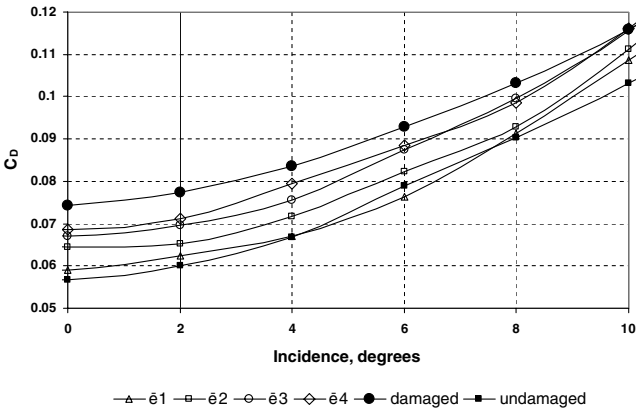

Fig. 32 Influence of repair thickness on C_D (square patch, full scheme).

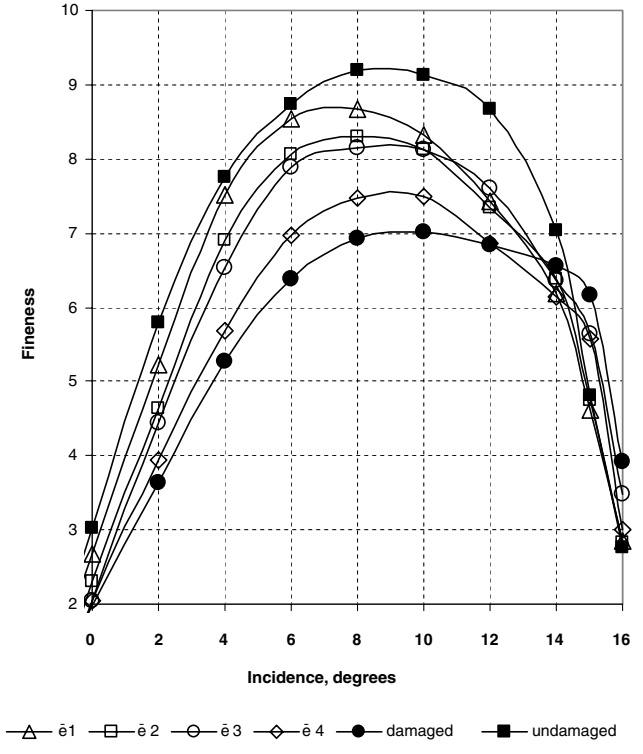

Fig. 33 Influence of repair thickness on the fineness (circular patch).

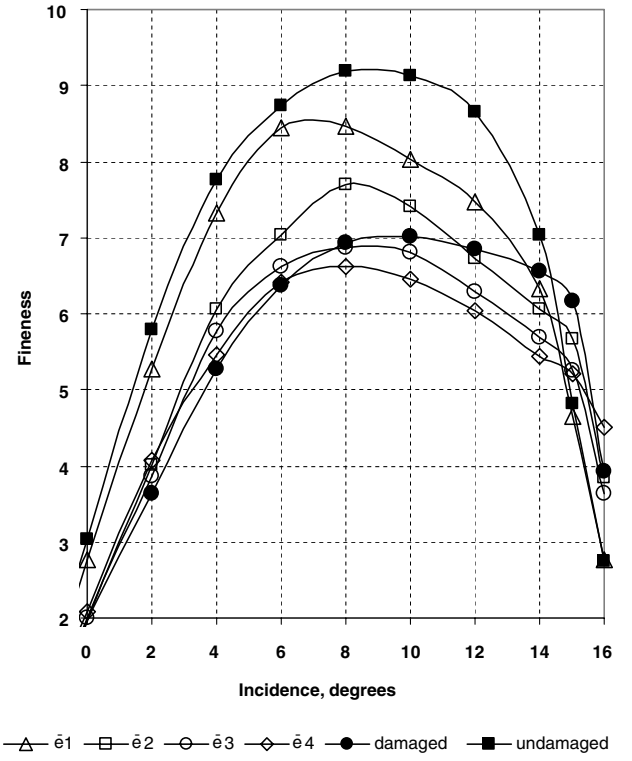

Fig. 34 Influence of repair thickness on the fineness (square patch).

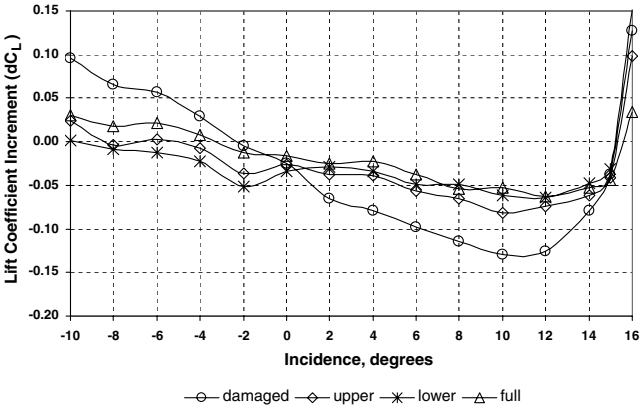

Fig. 35 Influence of the repair scheme on the increment of ΔC_L (position 1, circular patch, $e = 0.2$ mm).

or larger than 12 deg. For the circular patch (Fig. 45), the influence of the thickness on the improvements is not obvious for the three smallest values $\bar{e}_1$, $\bar{e}_2$, and $\bar{e}_3$ of $\bar{e}$. For these three thicknesses, there is on average almost a full recovery of C_D (compared with the undamaged state) for α not exceeding 8 deg, and beyond this value of α, the recovery decreases up until disappearing for 14 deg. In the case of the square patch (Fig. 46), the effect of the thickness on the improvements is quite clear. Thus, the smallest thickness $\bar{e}_1$ involves the best recovery of C_D and the improvement (or recovery) decreases then as the thickness increases. Such behavior is valid for α as large as 10 deg. For the smallest thickness $\bar{e}_1$, there is at 0 deg a recovery of 95% of the undamaged C_D (or an improvement of 25% from the damaged state) which reaches 100% (corresponding to an improvement of 15%) from 4 to 8 deg, and then decreases down to 94% (an improvement of 6% from the damaged state) for α increasing up to 12 deg. By comparison with C_L, as previously noticed, a complete recovery of C_D can be reached in the part of small incidence angles, whereas a full recovery cannot be reached for C_L.

Last but not least, in the case of fineness, for Figs. 47 and 48 (obtained in the same way as earlier for C_L and C_D), we notice trends

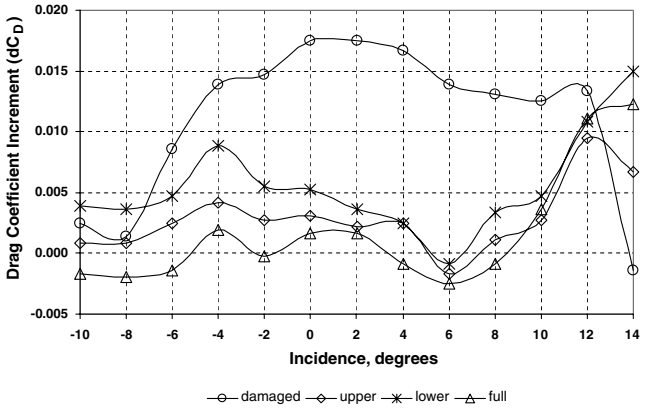

Fig. 36 Influence of the repair scheme on the increment of ΔC_L (position 1, circular patch, $e = 0.2$ mm).

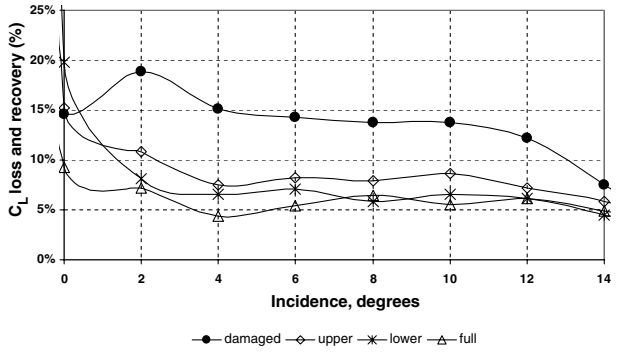

Fig. 37 Rate of loss and recoveries of C_L for different repair schemes (position 1, circular patch, $e = 0.2$ mm).

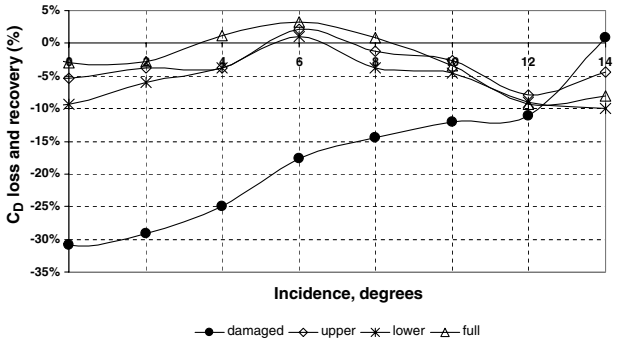

Fig. 38 Rate of loss and recoveries of C_D for different repair schemes (position 1, circular patch, $e = 0.2$ mm).

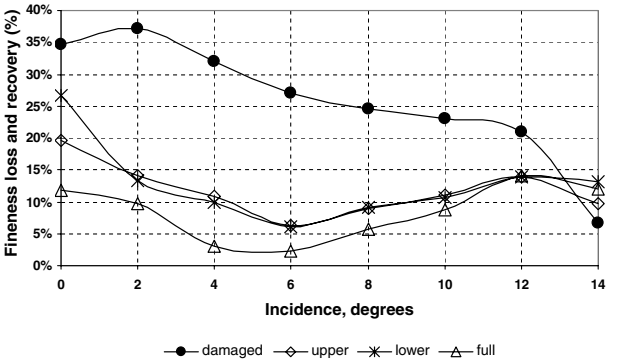

Fig. 39 Rate of loss and recoveries of f for different repair schemes (position 1, circular patch, $e = 0.2$ mm).

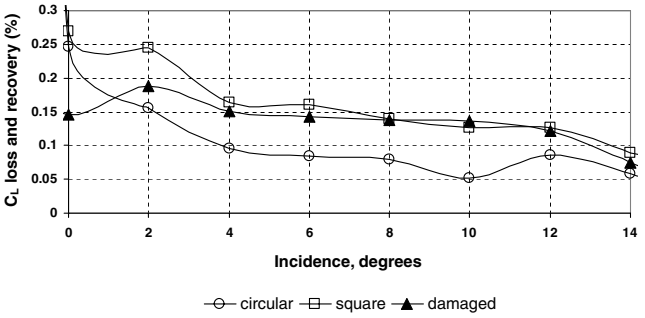

Fig. 40 Rate of loss and recoveries of C_L for different repair shape (position 1, full scheme, $e = 0.6$ mm).

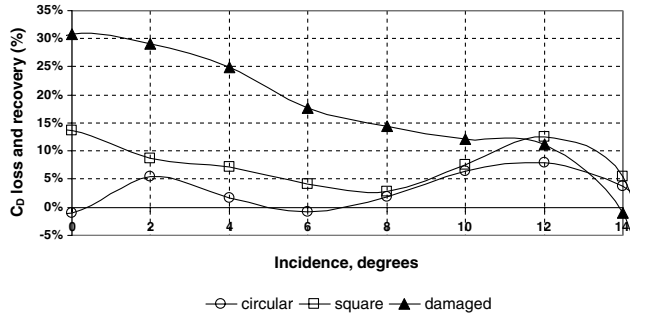

Fig. 41 Rate of loss and recoveries of C_D for different repair shape (position 1, full scheme, $e = 0.6$ mm).

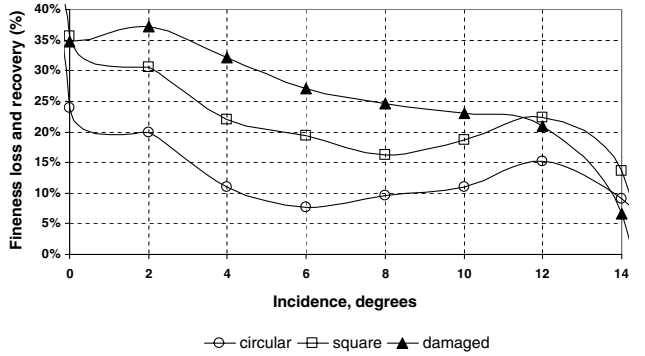

Fig. 42 Rate of loss and recoveries of f for different repair shape (position 1, full scheme, $e = 0.6$ mm).

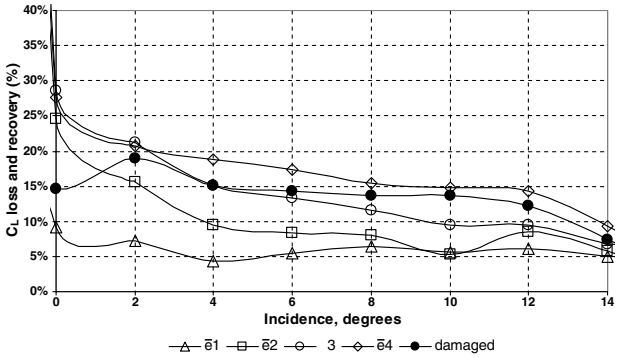

Fig. 43 Rate of loss and recoveries of C_L for different patch thicknesses (circular patch, full scheme).

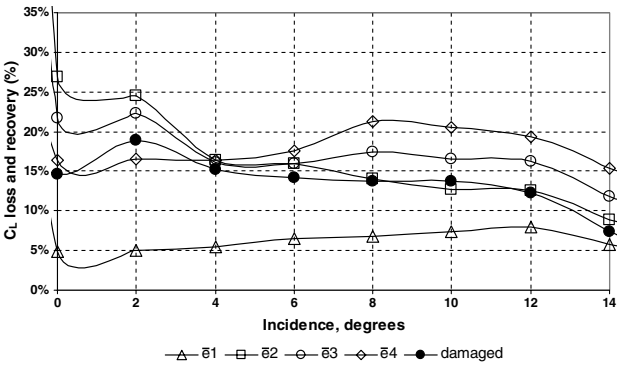

Fig. 44 Rate of loss and recoveries of C_L for different patch thicknesses (square patch, full scheme).

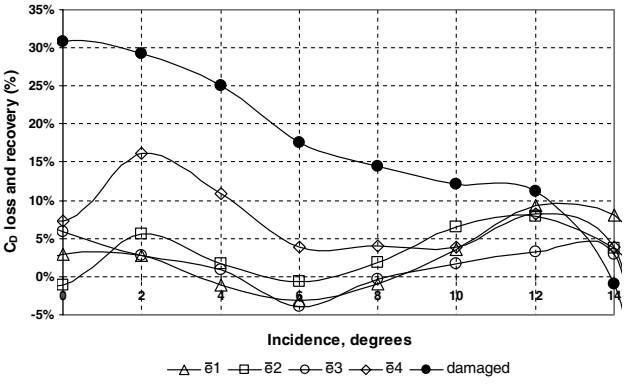

Fig. 45 Rate of loss and recoveries of C_D for different patch thicknesses (circular patch, full scheme).

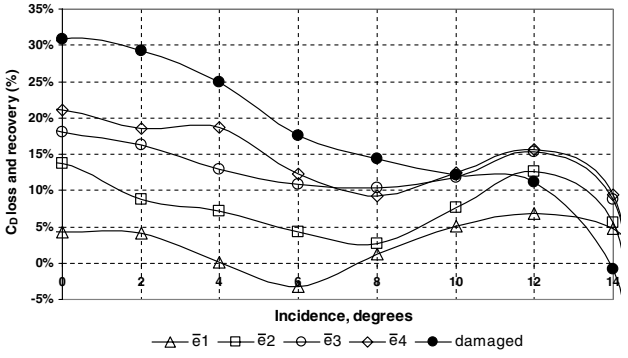

Fig. 46 Rate of loss and recoveries of C_D for different patch thicknesses (square patch, full scheme).

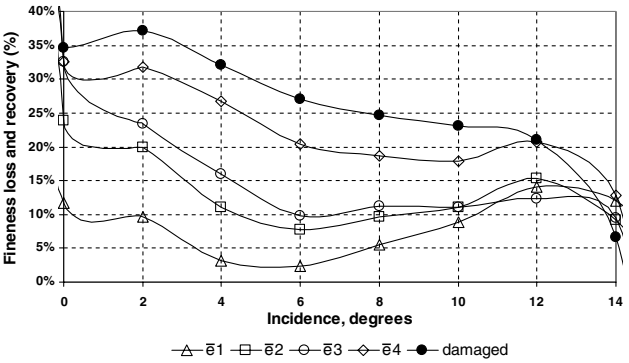

Fig. 47 Rate of loss and recoveries of the fineness for different patch thicknesses (circular patch, full scheme).

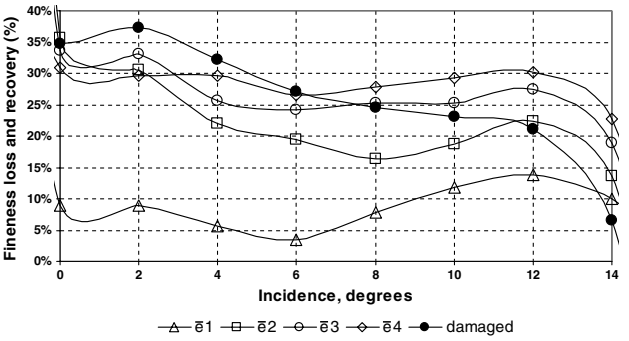

Fig. 48 Rate of loss and recoveries of the fineness for different patch thicknesses (square patch, full scheme).

of the effect of the thickness inverse of those of C_D when comparing the two shapes. That is to say, for the circular patch (Fig. 47), the effect of the thickness on the improvements is quite clear, whereas, in the case of the square patch, except the smallest thickness, the improvements are much more gathered. Indeed, for the two shapes, the effect of the thickness (or the improvement) decreases as $\bar{e}$ increases. Thus, the best recoveries are of course obtained with the smallest thickness $\bar{e}_1$. The circular and square patches appear to give almost the same improvements for this smallest value of thickness $\bar{e}_1$. This is not the case for the largest thicknesses $\bar{e}_2$, $\bar{e}_3$, and $\bar{e}_4$, where the improvements are better with the circular patch rather than the square patch. That is to say, when the patch is thick enough, the magnitude of the improvements of the initially degraded fineness depends on the shape of the patch, which is better when the patch is circular.

A first explanation of such differences between the square and circular shapes, provided the thickness of the patch is large enough, can be given by the configuration of the flow as indicated by Kind et al. [21], who indeed showed that a square patch with sharp edges fixed on a plate induces more important vortices shed from the lateral edges compared to a circular patch. This impinges on the drag coefficient which is increased as well [22].

VI. Conclusions

Experimental investigations have been conducted on both damaged and repaired wings of an aircraft model. For the first situation, it is shown that the presence of the damage induces a decrease of the lift and an increase of the drag. This means, in other words, a loss of the aerodynamic performances. This influence on the aerodynamic coefficients can be attributed to the flow through the hole which, on one hand, provokes a perturbation of the pressure distribution between the intrados and the extrados, and, on the other hand, produces an additional pressure drag. Visualizations consequently performed have indicated a link of this influence with the type of jet issuing from the damage hole.

Moreover, this investigation has also shown that the loss of performance increases when the damage size increases and when the damage location moves toward either the fuselage or the leading edge. It has been demonstrated that the ratio $\Delta C_D/\Delta S$ of the drag does not depend on the relative surface ΔS of the damaged hole, whereas the opposite is true in the case of the ratio $\Delta C_L/\Delta S$ of the lift. Finally, in terms of degradation (or loss), the lift coefficient appears to be more affected than the drag coefficient in most of the damage cases.

For the second part of this investigation, it is first shown that, for all the scheme repairs, the battle-damage repair patches can achieve substantial reductions in drag coefficient as well as increases in lift coefficient, close to those of the undamaged wing, depending on the incidence angle. Second, the full repair scheme appears, globally, to be more appropriate to gain aerodynamic performance lost from battle damage, provided that the patch is thin enough. Repairs of just one surface (upper or lower repairs) also produce significant improvements in lift and drag coefficients. The prevention of flow through the wing seems to be the major factor for the improvement.

Third, the increase of the patch thickness leads to the decrease of the improvement, so that, for large enough patch thickness, the repair does no longer lead to improvement; rather the opposite holds, relative to the unrepaired (unpatched) model. Consequently, repair by patches showed a compromise between the improvement due to the removal of flow through the damage hole and the performance loss due to the plates installed on the wings to remove the hole.

For all the schemes and the thicknesses, circular repair, as a more profiled shape, leads to better improvements than the square shape does. The square patch appears to be more sensitive to the increase of the patch thickness on the improvements, than the circular one. The full recovery can be achieved for the drag coefficient, whereas it is never reached for the lift coefficient for any scheme repair.

With the square patch in full repair scheme, the lift coefficient can decrease below the values of the damaged even for small incidence angle, which is not the case of the drag coefficient. Consequently, an addition of two square patches on both sides of an undamaged wing may provoke a decrease of the lift if the patches are thick enough.

According to the different results with the lift and the drag coefficients, the fineness appears to be a direct and better way to analyze the situation of the aerodynamic performances for the different cases investigated.

As a practical conclusion, to repair the battle-damaged surfaces on the wing, one just needs to use the full scheme with a circular patch, no matter the shape (square or circular), provided that the patch is thin enough, down to 0.3% of the local chord in the case of these investigations.

Acknowledgments

S. Djellal thanks P.M. Render from the Aeronautical and Automotive Department (Loughborough University, United Kingdom). The authors are also grateful for the help of H. Bouarroudj, A. Aissaoui, and C. Ghebache in manufacturing the model. The help of R. Lamara, A. Britah, and S. Ouazene in preparing and conducting tests is also gratefully acknowledged.

References

[1] Ball, R. E., *The Fundamentals of Aircraft Survivability Analysis and Design*, 2nd ed., AIAA Education Series, AIAA, Reston, VA, 2003.

[2] Irwin, A. J., "Investigation into the Aerodynamic Effects of Simulated Battle Damage to a Wing," Ph.D. Thesis, Aerodynamics and Automotive Dept., Loughborough Univ., Leicestershire, England, 1999.

[3] Irwin, A. J., and Render, P. M., "The Influence of Mid-Chord Battle Damage on the Aerodynamic Characteristics of Two-Dimensional Wings," *The Aeronautical Journal*, Vol. 104, No. 1033, 2000, pp. 153–161.

[4] Pitt, P., "Multiple-Site and Widespread Fatigue Damage in Aging Aircraft," *Engineering Failure Analysis*, Vol. 4, Dec. 1997, pp. 237–257.
doi:10.1016/S1350-6307(97)00020-4

[5] Jones, R., "Assessing and Maintaining Continued Airworthiness in the Presence of Wide Spread Fatigue Damage: An Australian Perspective," *Engineering Fracture Mechanics*, Vol. 60, No. 1, 1998, pp. 109–130.
doi:10.1016/S0013-7944(97)00021-0

[6] Jones, R., and Chui, W. K., "Composite Repairs to Cracks in Thick Metallic Components," *Composite Structures*, Vol. 44, Jan. 1999, pp. 17–29.
doi:10.1016/S0263-8223(98)00108-1

[7] Klug, J. C., and Sun, C. T., "Large Deflection Effects of Cracked Aluminium Plates Repaired with Bonded Composite Patches," *Composite Structures*, Vol. 42, July 1998, pp. 291–296.
doi:10.1016/S0263-8223(98)00018-X

[8] Seo, D. C., and Lee, J. J., "Fatigue Crack Growth Behaviour of Cracked Aluminium Plate Repaired with Composite Patch," *Composite Structures*, Vol. 57, July 2002, pp. 323–330.
doi:10.1016/S0263-8223(02)00095-8

[9] Avdelidis, N. P., Moropoulou, A., and Marioli Riga, Z. P., "The Technology of Composite Patches and Their Structural Reliability Inspection Using Infrared Imaging," *Progress in Aerospace Sciences*, Vol. 39, May 2003, pp. 317–328.
doi:10.1016/S0376-0421(03)00002-2

[10] Christian, F., Jr., Hammond, D. O., and Cochran, J. B., "Composite Material Repairs to Metallic Airframe Components," *Journal of Aircraft*, Vol. 29, No. 3, 1992, pp. 470–476.
doi:10.2514/3.46185

[11] Render, P. M., De Silva, S., Walton, A. J., and Mani, M., "Experimental Investigation into the Aerodynamics of Battle Damaged Airfoils," *Journal of Aircraft*, Vol. 44, No. 2, 2007, pp. 539–549.
doi:10.2514/1.24144

[12] Djellal, S., and Ouibrahim, A., "Conceptual Design of a Light Aircraft," *4èmes journées de Mécanique de l'EMP, JMEMP04*, Ecole Militaire Polytechnique, Algiers, Algeria, March 2004, pp. 60–66.

[13] Avery, J. G., "Design Manual for Impact Damage Tolerant Aircraft Structure," AGARD-AG-238Add, Oct. 1981.

[14] Mani, M., and Render, P. M., "Experimental Investigation into the Aerodynamic Effects of Airfoils with Triangular and Star Shaped Through Damage," AIAA Paper 2005-4978, June 2005.

[15] Robinson, K. W., and Leishman, J. G., "Effects of Ballistic Damage on the Aerodynamics of Helicopter Rotor Airfoils," *Journal of Aircraft*, Vol. 35, No. 5, 1998, pp. 695–703.
doi:10.2514/2.2379

[16] Irwin, A. J., Render, P. M., McGuirk, J. J., Probert, B., and Alonze, P. M., "Initial Investigation into the Aerodynamic Properties of a Battle Damaged Wing," *13th AIAA Applied Aerodynamics Conference*, AIAA Paper No. 95-1845, 1995.

[17] Render, P. M., and Walton, A. J., "Aerodynamics of Battle Damaged Wings: The Influence of Flaps, Camber and Repair Schemes," *23rd AIAA Aerodynamics Conference*, AIAA Paper 2005-4721, June 2005.

[18] "Lift-Interference and Blockage Corrections for Two Dimensional Subsonic Flow in Ventilated and Closed Wind Tunnels," IHS Engineering Sciences Data Unit, No. 76028, Nov. 1976.

[19] Mikolowsky, W., and McMahon, H., "An Experimental Investigation of a Jet Issuing from a Wing in Crossflow," *Journal of Aircraft*, Vol. 10, No. 9, 1973, pp. 546–553.
doi:10.2514/3.44390

[20] Rowley, C. W., Juttijudata, V., and Williams, D. R., "Cavity Flow Control Simulations and Experiments," *43rd AIAA Aerospace Sciences Meeting*, AIAA Paper 2005-0292, 2005.

[21] Kind, R. J., Black, K. J., and Carnegie, C. L., "A Preliminary Investigation of the Effects of Battle-Damage Repair Patches on the Aerodynamic Performance of a CF-18 Airfoil," *Canadian Aeronautics and Space Journal*, Vol. 44, June 1998, pp. 73–81.

[22] Gad-el-Hak, M., *Flow Control: Passive, Active and Reactive Flow Management*, Cambridge Univ. Press, Cambridge, London, U.K., 2000.